J. Marine Sci. Appl. (2011) 10: 377-393
DOI: 10.1007/s11804-011-1083-0

Comparative Analysis of the Separation Variation Influence on the Hydrodynamic Performance of a High Speed Trimaran

Khaled Hafez* **and Abdel-Rahman El-Kot**

Department of Naval Architecture and Marine Engineering, Faculty of Engineering, Alexandria University, Alexandria 21544 El-Shatbi, Egypt

Abstract: This paper numerically investigates the influence of separation variation of the outriggers on the hydrodynamic performance of a high speed trimaran (HST**)** aiming at improving its applicability in diverse realistic disciplines. The present investigation was performed within the framework of the 2-D slender body method (SBM) by calculating the resistance of three symmetric trimaran series moving in a calm free surface of deep water. Each trimaran series comprises of 4681 configurations generated by considering 151 staggers ($-50\% \le \alpha \le +100\%$), and 31 separations ($100\% \le \beta \le 400\%$) for 81 Froude numbers ($0.20 \le F_n \le 1.0$). In developing the three trimaran series, Wigley©-st, AMECRC©-09, and NPL©-4a models were used separately for both the main and side hulls of each individual series models. A computer macro named Tri-PL© was created using the Visual Basic for Applications©. Tri-PL© sequentially interfaced Maxsurf© then Hullspeed© to generate the models of the three trimaran series together with their detailed hydrostatic particulars, followed by their resistance components. The numerical results were partially validated against the available published numerical calculations and experimental results, to benchmark the Tri-PL© macro and hence to rely on the analysis outcomes. A graph template was created within the framework of SigmaPlot© to visualize the significant results of the Tri-PL© properly.

Keywords: high speed trimaran (HST); hydrodynamic interference factor (HIF); trimaran hydrodynamic performance; separation of outriggers
Article ID: 1671-9433(2011)04-0377-17

1 Introduction

Higher speeds require a significant reduction of wave-making resistance that is the most important component of ship resistance when the speed increases. To satisfy such a paradox, either higher values of slenderness ratio or higher dynamic lift of the hull is required. The last method appears to be unfavorable since, for a given speed, the lift-to-displacement ratio is reduced as the ship dimensions grow. Therefore, in order to design a high speed ship satisfying a certain speed shoulder at reasonable values of power, a slender hull must be used (Doctors, 1995).

As the size of the ship increases, the satisfactory slenderness ratio increases as well, up to a certain shoulder at which the hull stability becomes critical. At such critical stability, an imperative movement from mono-hulls to multi-hulls should be decided. The trimaran configuration, consisting of a slender central hull and two side hulls, seems to be a good solution (Hanhirova *et al*., 1995).

Having three separate slender hulls on a trimaran results in a higher wetted surface area comparing with a similar mono-hull or catamaran of similar displacement. At low speeds, this higher wetted surface area increases the frictional resistance and thus results in comparatively higher resistance. At high speeds, the wave-making resistance is relatively low due to the higher slenderness ratio. This is based on the widely accepted assumption that as the vehicle becomes finer the wave-making resistance decreases considerably. Also, wave-making resistance is affected by the interference between the wakes of the individual hulls. The appropriate position of the side hulls with respect to the main central hull results in a wake interference that certainly reduces this component of resistance. In other words, the favorable wave interference may compensate the increase of the wetted surface area ensuring the advantages of very slender hulls over a significant range of F_n. In fact, the combination of a slender hull form and the appropriate position of side hulls may result in a considerable resistance reduction at higher speeds together with acceptable stability characteristics compared to both mono-hulls and catamarans.

Many of the today's high-speed trimarans have transom sterns of different configurations and extents, which violate the conventional simple hydrodynamic analysis (Doctors and Day, 1997; Robards and Doctors, 2003), (Doctors and Beck, 2005; Doctors, 2006; Doctors, 2006). Proper analysis of the hydrodynamic problems associating transom sterns would require a full 3-D manipulation which is not an easy task and a very time consuming issue. In this regard, the present 2-D study allows the performance of high speed

Received date: 2011-07-12.
***Corresponding author Email:** kamhjp@lycos.com

trimarans to be investigated and provides some practical trimaran resistance data for use at the preliminary design stage.

Although, the overall calm water resistance components against which the trimaran may be designed to withstand is as shown in Fig.1, this research doesn't consider the overstrike components.

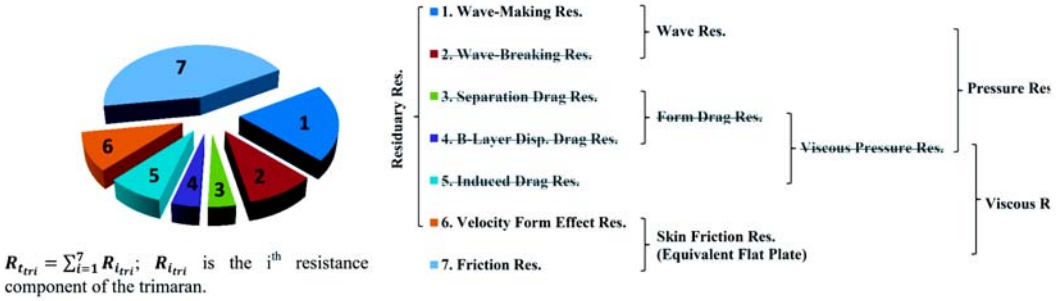

Fig.1 Components of Calm Water Resistance

2 Theoretical background

This section is prepared to introduce a brief theoretical background on the hydrodynamic theories upon which the adopted computational computer programs are based. The subject matter is introduced primarily for its practical importance, tempered by the limitations of space and complexity that may be tolerated in a research paper.

2.1 2-D SBM of HullSpeed©

The slender body method (SBM) of the HullSpeed© (2011), as an analytical method, calculates the wave resistance of a slender marine vehicle by calculating the energy in the vehicle-induced free surface wave pattern and thus its wave resistance. In the SBM a potential non-lifting model with linearized free surface conditions for calculating the wave pattern and hence the wave resistance of a body moving at high-speed in a free surface of a finite depth channel is adopted. The hull is discretized into a large number of quadrilateral panels, and with the source singularities they are then placed adjacent to each panel center forming a planar array along the ship's central plane. The fundamentals behind the theory involve obtaining the source strength as a function of the longitudinal deviation of the hull. The source strengths depend only on the local panel slope and calculated independently of each other; the source strength on a panel of the hull is calculated from the panel normal. The wave resistance is acquired by integrating the forward and aft components of the pressure normal to the body over the surface of the hull, where the apparent pressure around the body that causes disturbance in the free surface is dictated from the flow around the body.

Multi-hull vessels may be represented by a number of source arrays, one for each hull, placed at the required positions in the channel. The wave resistance of the sources is calculated from an expression derived by Insel (1990) which describes the resistance in terms of the far-field Eggers coefficients (Eggers, 1955) for a source in a finite channel not from pressure integration over the hull. The resistance of the sources is dependent on the number of the wave harmonics; to obtain the total wave pattern resistance, approximately 100–150 harmonics should be used. The wave number and the wave angle of the *i*th harmonic satisfy the wave speed condition including shallow water effects and the wall reflection condition.

Most slender body methods omit sources on the transom. This is due to the fact that the waterline slope is undefined on the transom. If the model is not closed at the stern, then there is a source deficit which causes the resistance to be under-predicted when compared with experimental measurements of wave pattern resistance. Several methods for making up this resistance deficit have been developed by various researchers, including a hydrostatic correction, a transom source-correction and a virtual appendage approach (Tuck *et al*., 1999) and (Couser *et al*. 1998).

Concerning the virtual appendage approach for making up this resistance deficit, it involves the addition of a virtual appendage to the transom which encloses the separated flow in the low speed range and the air pocket in the high speed range. The horizontal planar flow around the transom may be considered by examining the 2-D flow over a backward facing step. It is noted by Batchelor (1959) and Sinha (1981) that the streamline re-attachment length behind the step tends to 6 times the step height for high Reynolds number turbulent flow. In this manner the transom stern body is closed by the addition of an extra point downstream of the transom for each water line; the downstream offset (reattachment length) being 6 times the transom half-breadth. It is possible to optimize the predictions by varying the re-attachment length slightly. In fact, SBM calculates the wave resistance coefficients and wave patterns with fine details efficiently over a short computational time span.

2.2 2-D Thin ship theory (TST) of Michlet©

The thin ship theory (TST), upon which Michlet© (2010) is based, was introduced by Michell (1898) as a purely

analytical approach for calculating the wave resistance of a thin marine vehicle. The essential assumption is that the hull is thin, i.e. the beam is small compared to all other characteristic lengths of the hull.

There are two mathematical simplifications that are introduced in TST. The major simplification is that, which is common to all linear theories, the kinematic and dynamic free-surface boundary conditions may be approximated by a linearized "Kelvin" condition on the plane equilibrium surface. The second simplification is that the body boundary condition, i.e. the disturbance to the flow, which is created by the immersed hull, may be approximated by a continuous distribution of source singularities of predetermined magnitude along the central-plane of the thin hull and of strength expressed in terms of the hull geometry. The necessary source potential that satisfies the free-surface boundary condition is a complicated function that must possess an asymptotic approximation far downstream of the same form as the Kelvin wave system, with the velocity potential locally a plane wave. In addition, this source potential must depend in a suitably symmetrical manner on the position of the source and of the field point where the potential is measured (Newman, 1999), (Wehausen, 1971) and (Wehausen and Laitone, 1960).

Validating the numerical results of the TST against the experimental results shows a reasonable agreement at higher F_n, whereas TST exaggerates the interference effects at lower F_n. A common explanation for this discrepancy is that viscous effects suppress the interference effects in a real fluid. An alternative possibility results from the fundamental assumption of the TST that the beam is small compared to all other characteristic lengths of the hull. The wavelength is significant in this context and should be recognized as an additional length scale not present in the steady-state lifting-surface problem. Since the wave length is proportional to the ship's speed squared, it is inevitable that the Michell approximation will break down at a lower F_n.

In the TST, there exists a small non-reducible error due to the thin hull representation which allows a small volume of fluid to enter the hull near the bow and exit it near the stern, the effect of which is to under-represent the hull, resulting in a smaller disturbance to the flow, and hence the free surface, than would otherwise be expected.

2.3 3-D Panel method of ShipFlow©

ShipFlow© (2011), as computational fluid dynamics (CFD) software, calculates ship hull resistance (both viscous and wave components), development of the wave profiles and consequential matters, such as trim and sinkage characteristics, and the changes in velocities and pressure field around appendages, such as the propellers. Some of these problems remain a challenge to researchers in order to produce a sufficiently reliable CFD program to handle the complex phenomenon of fluid and object interactions. ShipFlow© (2011) uses panel methods to define the free surface, hull(s), and transom(s), if any, that are to be considered in calculating the wave resistance coefficients.

As a free stream flow past a marine vehicle, the laminar flow starts from the stagnation point, diverges gradually as it moves downstream, and when it reaches the transition point where the viscous force is insufficiently strong to bond the streamlines, it breaks down and become turbulent. Therefore, ShipFlow© (2011) calculates the wave resistance of a marine vehicle by splitting the flow past it into three regions (Newman, 1999).

The first region includes the fluid flow in the outermost area and follows the potential flow theory. In this region the flow is calculated using a higher order panel (HOP) method, also known as the Rankin panel source (RPS) method. The fluid flow is treated as continuous streamlines starting from the forward end of the ship (bow), and extending back to its aft end (stern), assuming that the flow is steady, incompressible, and irrotational.

The second region includes thin boundary layers along the ship hull and follows the boundary layer theory. In this region the flow is calculated using a 3-D momentum integral (3DMI) method. This region starts at the bow stagnation point(s) and continues along the surface of the hull, including the flow in the corresponding laminar, laminar-to-turbulent transition, and turbulent zones.

The third region is fully turbulent, includes the wake, and follows the Navier-Stokes theory. In this region the Reynolds-Average Navier-Stokes (RANS) method is used to calculate the energy and the adverse resistance at the stern region of the hull. The majority of the wave resistance is obtained using this method, as the interference between the viscous boundary layers of this region is calculated.

The assumptions that the fluid is incompressible and Newtonian allow for simplification of the fundamental equations for hydrodynamic applications. So the continuity equation and the subsequent conservation-of-momentum equations are all that are required in order to solve for the velocity and pressure fields of an incompressible flow. ShipFlow© (2011) calculates the wave resistance coefficients efficiently considering the price of long computational time. However, as F_n increases, ShipFlow© (2011) becomes increasingly unstable in its ability to model transom spray and wave breaking phenomena.

3 Generated model series

The first critical step in this research is to select appropriate hull forms upon which a realistic trimaran model may be configured. In this regard, three well known slender models,

namely Wigley©-st (Wigley, 1934), AMECRC©-09 (Bojovic, 1995) and (Bojovic and Goetz, 1996), and NPL©-4a (Marwood and Bailey, 1969) and (Bailey, 1976) are used separately in developing both the main and side hulls of three symmetric trimaran series. Each series comprises of 4681 configurations generated by considering 151 staggers covering the interval $-50\% \le \alpha \le +100\%$, and 31 separations covering the interval $100\% \le \beta \le 400\%$ for 81 Froude numbers covering the interval $0.20 \le F_n \le 1.0$. Figs.2–4 show the geometric configurations of the aforementioned parent models, respectively, while the name of each parent model is used for referencing the corresponding trimaran. The principal particulars of the main and side hulls of the Wigley©-st, AMECRC©-09, and NPL©-4a trimarans are tabulated in Table 1.

Table 1 Principal Particulars of the Wigley©-st, AMECRC©-09 and NPL©-4a Trimarans

Design parameter	Wigley©-st		AMECRC©-09		NPL©-4a	
	Main hull	Side hull	Main hull	Side hull	Main hull	Side hull
L_W/m	50.0000	25.0000	50.0000	25.0000	50.0000	25.0000
B_W/m	5.0000	2.5000	6.2530	3.1265	5.5730	2.7865
D_M/m	6.2500	3.1250	7.4000	3.7000	6.2610	3.1305
d_M/m	3.1250	1.5625	2.5000	1.2500	2.7850	1.3925
C_B	0.4440		0.4990		0.3940	
C_P	0.6670		0.6210		0.6840	
C_M	0.6670		0.8110		0.6550	
C_W	0.6670		0.7930		0.7600	
Δ / t	355.9000	44.4876	400.2000	50.0248	313.6000	39.2000
A_S /m^2	371.9660	92.9915	365.8430	91.4608	330.3620	82.5905
A_M /m^2	10.4160	2.6040	12.5650	3.1413	8.9400	2.2350
A_W /m^2	166.6620	41.6655	248.0010	62.0002	211.8380	52.9595
LCB /(%L_W)	50.0000 (ford Aft Perp.)		44.5620 (ford Aft Perp.)		43.6840 (ford Aft Perp.)	
LCF /(%L_W)	50.0000 (ford Aft Perp.)		41.1550 (ford Aft Perp.)		41.7320 (ford Aft Perp.)	
KB /m	1.9530	0.9765	1.5730	0.7865	1.9250	0.9625
BM_T /m	0.6860	0.3430	1.7380	0.8690	1.3890	0.6945
BM_L /m	60.0030	30.0015	97.2330	48.6165	103.5550	51.7775
*MCT*1.0cm/(t·m)	1.7080	0.4270	2.5420	0.6355	2.1710	0.54275
L_W / $\nabla^{1/3}$	4.4100	0.5513	7.9080	0.9885	6.6150	0.8269
TPC/ (t/cm)	7.1138		6.8410		7.4203	
L_W /B_W	10.0000		7.9962		8.9718	
B_M/d_M	1.6000		2.5012		2.0011	
λ	1.0000	0.5000	1.0000	0.5000	1.0000	0.5000

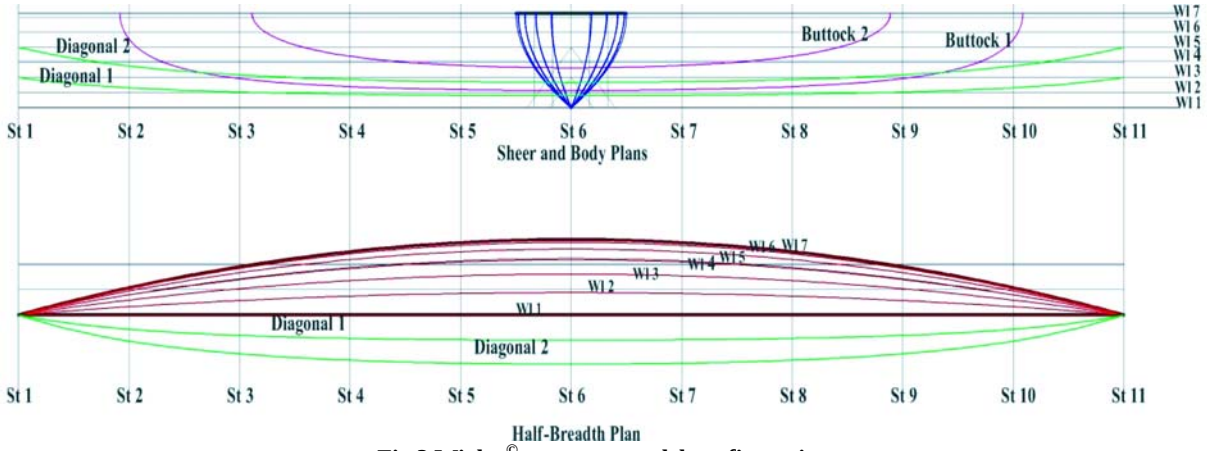

Fig.2 Wigley©-st parent model configuration

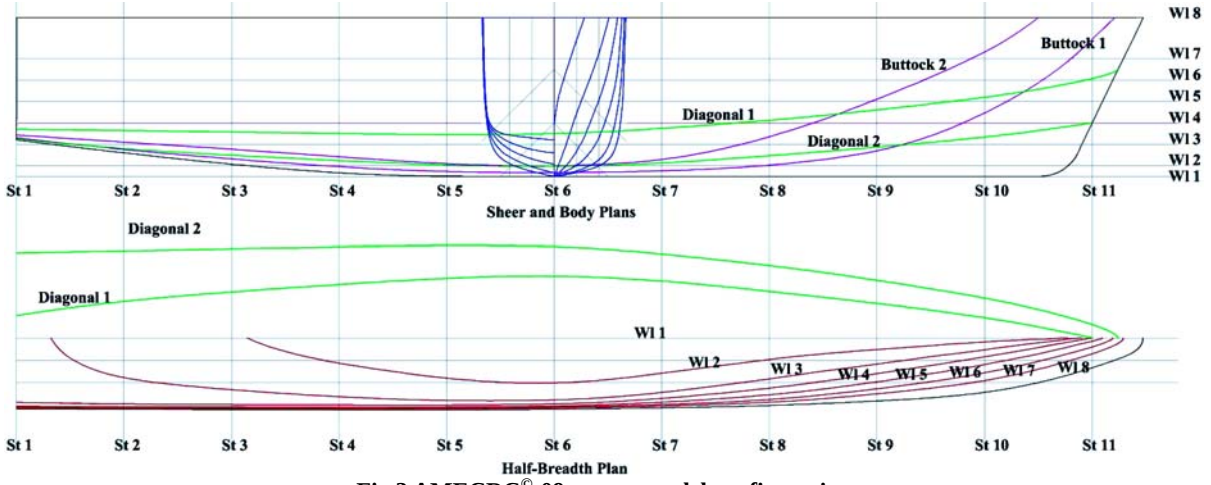

Fig.3 AMECRC©-09 parent model configuration

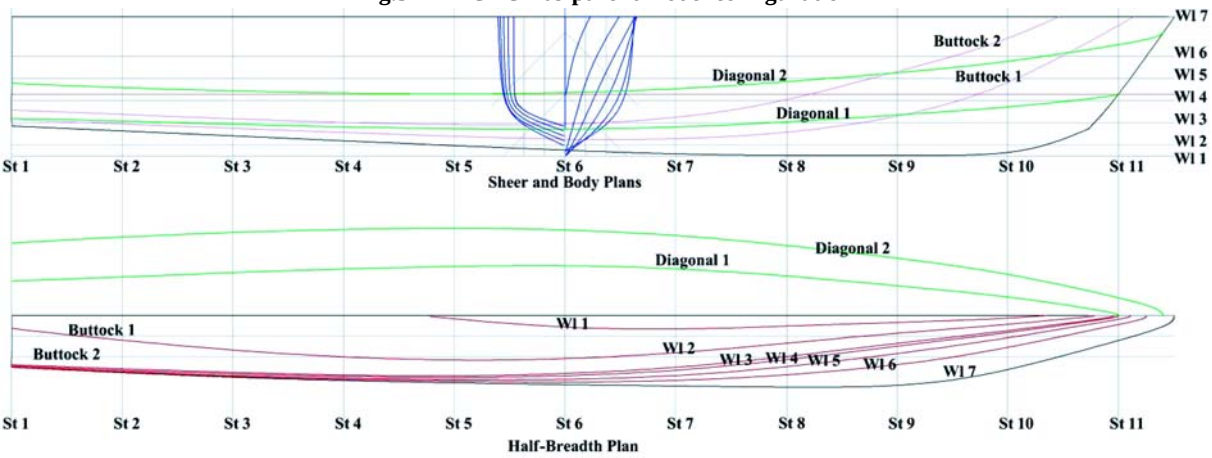

Fig. 4 NPL©-4a parent model configuration

The idea behind which Wigley©-st, AMECRC©-09, and NPL©-4a models are used in the present research is not only due to the availability of the numerical and experimental data describing the flow around them, but also due to a few important hydrodynamic reasons.

Concerning the Wigley©-st model, as it has a parabolic form $\left(\theta_E = 10.5^\circ\right)$, it may be modeled exactly in Maxsurf©, and therefore any deviation in its geometrical configuration, and/or in its numerical results may be well recognized and interpreted. Also, the Wigley©-st model has a thin and sharp bottom $\left(\theta_D = 38.5^\circ\right)$, bow, and stern with its insensitivity to the pressure fields at such regions. In addition, Wigley©-st is a non-transom model, and therefore the hydrodynamic problems associating the transom-stern; i.e., the vague vertices formation at higher F_n, the flow unsteadiness, and the apparent spray pattern (rooster tail) on the free surface behind the model do not exist.

Concerning the AMECRC©-09 model, it is designed for operation at $0.10 \le F_n \le 1.0$, and LCB positioned in the aft body. The hull form is characterized by a fairly rounded entrance waterline $\left(\theta_E = 13^\circ\right)$, almost V-type bow sections except a shallow flare at the far ford section, rounded aft body sections, straight buttock lines terminating smoothly at the transom, and shallower dead-rise $\left(\theta_D = 13^\circ\right)$.

Concerning the NPL©-4a model, it is designed for operation at $0.30 \le F_n \le 1.20$, and LCB positioned in the aft body. The hull form is characterized by straight entrance waterlines $\left(\theta_E = 11^\circ\right)$, apparent flared bow sections near the design waterline, rounded aft body sections, straight buttock lines terminating sharply at the transom, and significant bottom dead-rise $\left(\theta_D = 32.5^\circ\right)$.

4 Coordinate system and notations

In the Maxsurf© (2011) package and its downstream analysis modules, a right-handed trimaran-fixed coordinate system is used. The positive directions of such coordinate systems are arbitrarily selected to be forward for the longitudinal axis x, starboard side for the transverse axis y, and up for the vertical axis z, with their origin arbitrarily positioned at the intersection of the aft perpendicular with the central longitudinal plane of the main hull. Fig.5 shows the schematic view of the coordinate

system and dimensional notation of the analysis trimaran. In the present investigation, α and β are expressed as percentages of L_W and B_W, respectively, as given in equations (1 and 2).

$$\alpha = x/L_W \cdot 100 \tag{1}$$

$$\beta = y/B_W \cdot 100 \tag{2}$$

5 Resistance calculations

The resistance calculation adopted in this investigation is based on the SBM embedded in the Hullspeed© (2011), which in turn is based on the work of Tuck *et al*. (1999) and Couser *et al*. (1998). Such methods calculate the ship energy dissipated in generating the free surface wave pattern, and hence the wave-making resistance of a symmetric vehicle. In applying the SBM, hulls with transom sterns are dealt with by automatically adding a virtual appendage, which is not the case with the non-transom stern hulls. Figs.6–8 show the slender body mesh for Wigley©-st, AMECRC©-09, and NPL©-4a symmetric trimarans all at $\alpha = +5\%$ and $\beta = 200\%$ for mesh sizes $m \times n = 81 \times 16$, 81×13, and 81×14, respectively. The influence of both parallel sinkage and trim of the trimarans, as well as the planning forces which limit the speed range applicability of the SBM are not considered in this investigation.

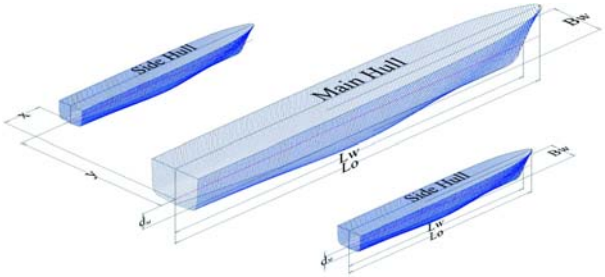

Fig.5 Schematic view of the coordinate system and dimensional notation of the analysis trimaran

Hullspeed© breaks down $R_{t_{tri}}$ into the two conventional components which scale according to different resistance laws; Froude number dependent component, e.g. $R_{w_{tri}}$ or $R_{r_{tri}}$, and a Reynolds number dependent component, e.g.. $R_{v_{tri}}$ or $R_{f_{tri}}$.

In terms of coefficients, and neglecting the wave-breaking, eddy and appendage resistances, the calm water total resistance of a trimaran may be expressed as given in equations (3 or 4).

$$C_{t_{tri}} = C_{w_{tri}} + C_{v_{tri}} + C_{a_{tri}} \tag{3}$$

$$C_{t_{tri}} = C_{r_{tri}} + C_{f_{tri}} + C_{a_{tri}} \tag{4}$$

where $C_{a_{tri}} = 0.0004$ is adopted throughout the present numerical calculations (1957).

In terms of the standard notation, the individual components of the trimaran calm water resistance coefficients may be represented as given in Eqs.(5)–(8) respectively.

$$C_{w_{tri}} = R_{w_{tri}}/0.5\rho A_{S_{tri}} U^2 \tag{5}$$

$$C_{v_{tri}} = R_{v_{tri}}/0.5\rho A_{S_{tri}} U^2 \tag{6}$$

$$C_{r_{tri}} = R_{r_{tri}}/0.5\rho A_{S_{tri}} U^2 \tag{7}$$

$$C_{f_{tri}} = R_{f_{tri}}/0.5\rho A_{S_{tri}} U^2 \tag{8}$$

Fig.6 Slender body mesh for Wigley©-st symmetric trimaran at $\alpha = +5\%$ and $\beta = 200\%$ for $m \times n = 81 \times 16$

Fig.7 Slender body mesh for AMECRC©-09 symmetric trimaran at $\alpha = +5\%$ and $\beta = 200\%$ for $m \times n = 81 \times 13$

Fig.8 Slender body mesh for NPL©-4a symmetric trimaran at $\alpha = +5\%$ and $\beta = 200\%$ for $m \times n = 81 \times 14$

The calm water friction resistance coefficient of the non-interfered trimaran hulls $C_{f_{tri-NI}}$ may be calculated as given in Eq.(9).

$$C_{f_{tri-NI}} = \left(1/A_{S_{tri}}\right) \cdot \left[A_{S_{cnt}} C_{f_{cnt}} + 2 A_{S_{out}} C_{f_{out}}\right] \tag{9}$$

The wetted surface area of the trimaran $A_{S_{tri}}$ may be expressed as given in Eq.(10).

$$A_{S_{tri}} = A_{S_{cnt}} + 2 A_{S_{out}} \tag{10}$$

The calm water friction resistance coefficients $C_{f_{cnt}}$ and $C_{f_{out}}$ may be calculated approximately using the ITTC'57 (1957) turbulent correlation line as given in equations 11 and 12, respectively.

$$C_{f_{cnt}} = 0.075/\left(\log_{10} R_{e_{cnt}} - 2\right)^2 \tag{11}$$

$$C_{f_{out}} = 0.075/\left(\log_{10} R_{e_{out}} - 2\right)^2 \tag{12}$$

where the ITTC'57 salt water properties are $\varepsilon = 3.5\%$, $t = 15^{\circ}$, $\rho = 1025.90\,kg/m^3$ and $\nu = 1.18831\times10^{-6}\,m^2/s$.

The Reynolds numbers $R_{e_{cnt}}$ and $R_{e_{out}}$ may be calculated as given in equations 13 and 14, respectively.

$$R_{e_{cnt}} = U\,L_{W_{cnt}}/\nu \tag{13}$$

$$R_{e_{out}} = U\,L_{W_{out}}/\nu \tag{14}$$

The calm water viscous resistance of the non-interfered trimaran hulls $C_{v_{tri-NI}}$ includes a form effect applied to the frictional resistance of the individual hulls, and may be calculated as given in equations 15 and 16.

$$C_{v_{tri-NI}} = \left(1/A_{S_{tri}}\right)\cdot\left[A_{S_{cnt}}C_{v_{cnt}} + 2A_{S_{out}}C_{v_{out}}\right] \tag{15}$$

$$C_{v_{tri-NI}} = \left(1/A_{S_{tri}}\right)\cdot\left[A_{S_{cnt}}(1+k)_{cnt}C_{f_{cnt}} + 2A_{S_{out}}(1+k)_{out}C_{f_{out}}\right] \tag{16}$$

Where $(1+k)_{cnt}$ and $(1+k)_{out}$ reflect the 3-D form effect of the main and side hulls as well as the viscous interaction effects between the triple hulls constituting the trimaran, and may be estimated using an empirical formula.

The calm water wave-making resistance coefficient of the non-interfered trimaran hulls $C_{w_{tri-NI}}$ may be calculated as given in Eq.(17).

$$C_{w_{tri-NI}} = \left(1/A_{S_{tri}}\right)\cdot\left[A_{S_{cnt}}C_{w_{cnt}} + 2A_{S_{out}}C_{w_{out}}\right] \tag{17}$$

The calm water residuary resistance coefficient of the non-interfered trimaran hulls $C_{r_{tri-NI}}$ may be calculated as given in Eq(18).

$$C_{r_{tri-NI}} = C_{w_{tri-NI}} + \left(1/A_{S_{tri}}\right)\cdot\left[A_{S_{cnt}}k_{cnt}C_{f_{cnt}} + 2A_{S_{out}}k_{out}C_{f_{out}}\right] \tag{18}$$

Combining Eqs.(9) and (17), then the calm water total resistance coefficient of the non-interfered trimaran hulls $C_{t_{tri-NI}}$ may be calculated as given in Eq.(19).

$$C_{t_{tri-NI}} = \left(1/A_{S_{tri}}\right)\cdot\left[A_{S_{cnt}}C_{t_{cnt}} + 2A_{S_{out}}C_{t_{out}}\right] \tag{19}$$

6 Interference factor (η)

The calm water resistance of the bonded trimaran drastically varies from that of the non-interfered trimaran hulls. To evaluate the hydrodynamic interference effects of the individual design configurations, the interference factor η may be calculated as the difference in total resistance captured when moving from separate triple hulls into one bonded trimaran. It is convenient to express such difference as a ratio of the non-interfered total resistance as given in equation (20).

$$\eta = C_{t_{tri}}/C_{t_{tri-NI}} - 1.0 \tag{20}$$

A negative interference factor indicates a beneficial interference; i.e., the resistance of the trimaran configuration is less than the summed individual resistances of the triple hulls, whereas a positive interference factor implies the existence of a detrimental interference.

7 Automation and programming implementation

The Maxsurf© (2011) CAD package and its downstream analysis modules provide direct automation support that allows the interested user to create, modify, and analyze many design models over a minimum time span. None of the Maxsurf© (2011) modules include an embedded environment to write or record macros, but they accept their interface via the conventional programming languages, e. g., Visual C^{++}©, Visual Basic©, Visual FORTRAN©, Java©, or Microsoft© Windows© Scripting Host©, etc. Also, all Maxsurf© (2011) modules have the ability to interface spreadsheet applications such as Microsoft© Excel©, other CAD systems such as Autodesk© AutoCAD©, and other graphing systems such as SigmaPlot©, to either get more design details or to get more visualization quality.

Seeking automation of the rigorous resistance calculation procedures of the three trimaran series, a sophisticated computer macro named Tri-PL© is developed from scratch based on Visual Basic for Applications© (2010). To generate each model of the three individual trimaran series together with its detailed hydrostatic particulars, Tri-PL© automatically interfaces with the Maxsurf© (2011) module. To calculate the resistance components for each model of the three individual trimaran series, Tri-PL© automatically interfaces with the Hullspeed© (2011) module. To visualize the significant analysis results of the Tri-PL© properly, a graph template of the SigmaPlot© (2006) is created. Fig.9 depicts the algorithm of the resistance calculations for the Wigley©-st, AMECRC©-09, and NPL©-4a trimaran series.

The time necessary for generating each of the three individual trimaran series of Wigley©-st, AMECRC©-09, and NPL©-4a together with the detailed calculation of the hydrostatic particulars, resistance, and data visualization is about 21000*CPU* seconds on an Intel© i5-2.40 GHz, 3.0 MB cash, and 4.0 GB DDR3 Dell© Inspiron-1545 Laptop.

8 Validation and benchmarking

Both Wigley©-st and AMECRC©-09 models are selected to validate the accuracy and homogeneity of the SBM numerical results, as well as benchmark the newly developed

computer macro Tri-PL©. For the validation purposes only, the scale ratio of the side-to-main hulls of Wigley©-st and AMECRC©-09 models are $\lambda = 0.500$ and $\lambda = 0.459$, respectively.

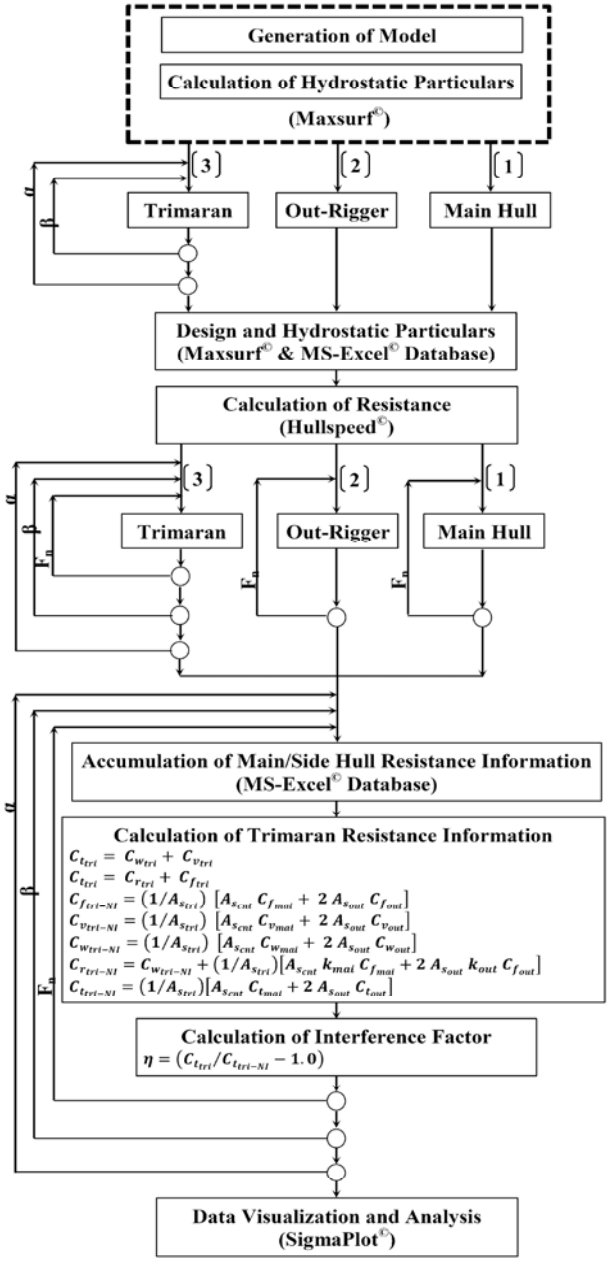

Fig.9 Algorithm of the resistance calculations for Wigley©-st, AMECRC©-09 and NPL©-4a trimaran series

Fig.10 shows the variation of $C_{w_{tri}}$ versus F_n for one Wigley©-st symmetric trimaran model corresponding to $\alpha = 0\%$ and $\beta = 131.24\%\%$, calculated by both the Michlet© (2010) computer program and Hullspeed© (2011) via the Tri-PL© macro. In such validation, the numerical results of Hullspeed© (2011) via the Tri-PL© macro seem to agree very well with those of Michlet© (2010), and both confirm the validation of Hullspeed© (2011).

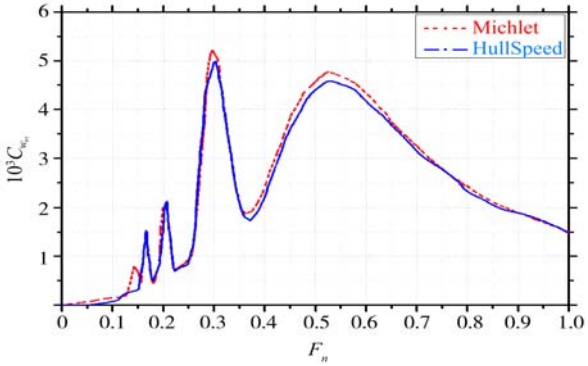

Fig.10 Validation of $C_{w_{tri}}$ versus F_n for the Wigley©-st symmetric trimaran at $\alpha = 0\%$ and $\beta = 131.60\%$, for $m \times n = 81 \times 16$

Fig.11 shows the variation of $C_{w_{tri}}$ versus F_n for three AMECRC©-09 symmetric trimaran models corresponding to $\alpha = -20\%$, -30% and -40% all at $\beta = 160\%$, predicted by four methods.

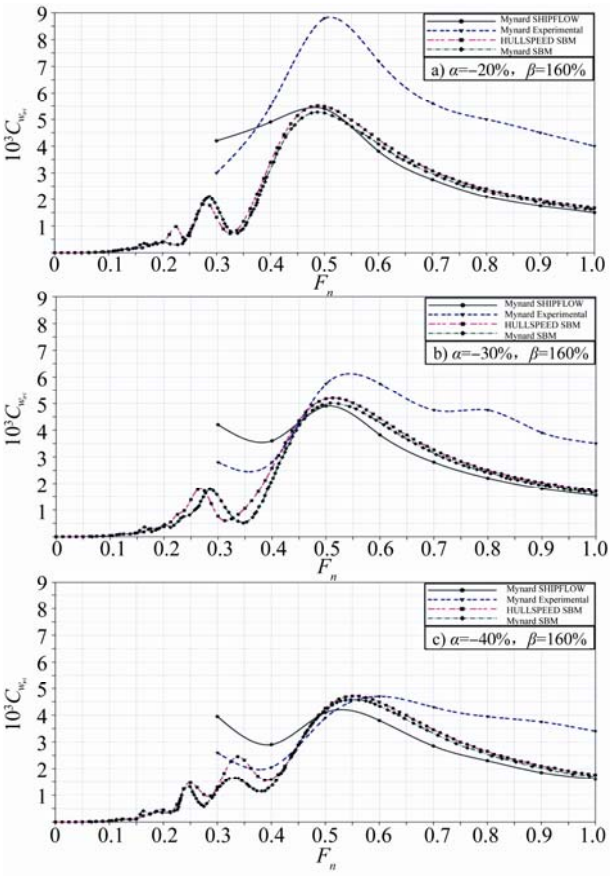

(a) $\alpha = -20\%$, $\beta = 160\%$
(b) $\alpha = -30\%$, $\beta = 160\%$
(c) $\alpha = -40\%$, $\beta = 160\%$

Fig.11 Validation of $C_{w_{tri}}$ versus F_n for the AMECRC©-09 symmetric trimaran for $m \times n = 81 \times 13$

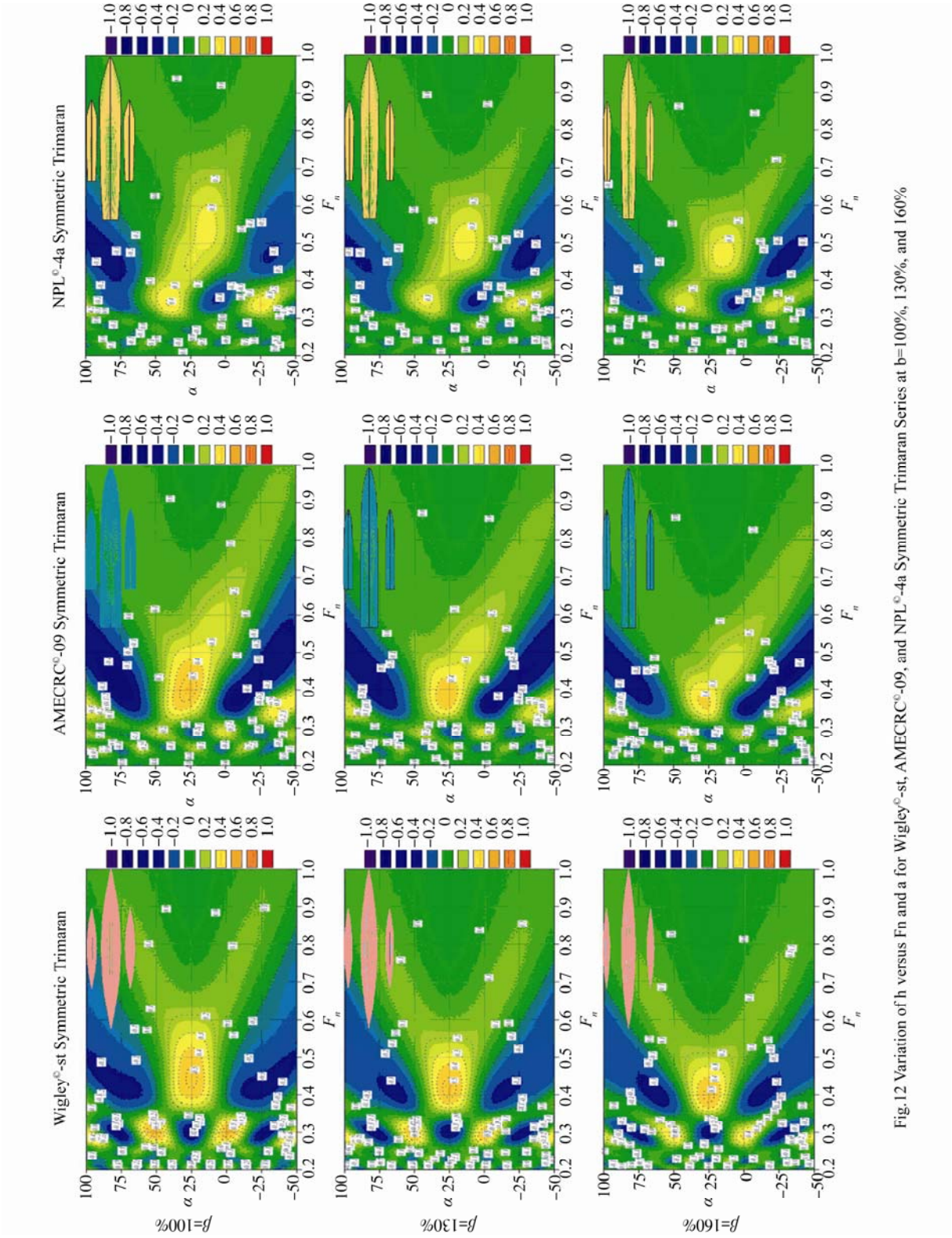

Fig.12 Variation of h versus Fn and a for Wigley©-st, AMECRC©-09, and NPL©-4a Symmetric Trimaran Series at b=100%, 130%, and 160%

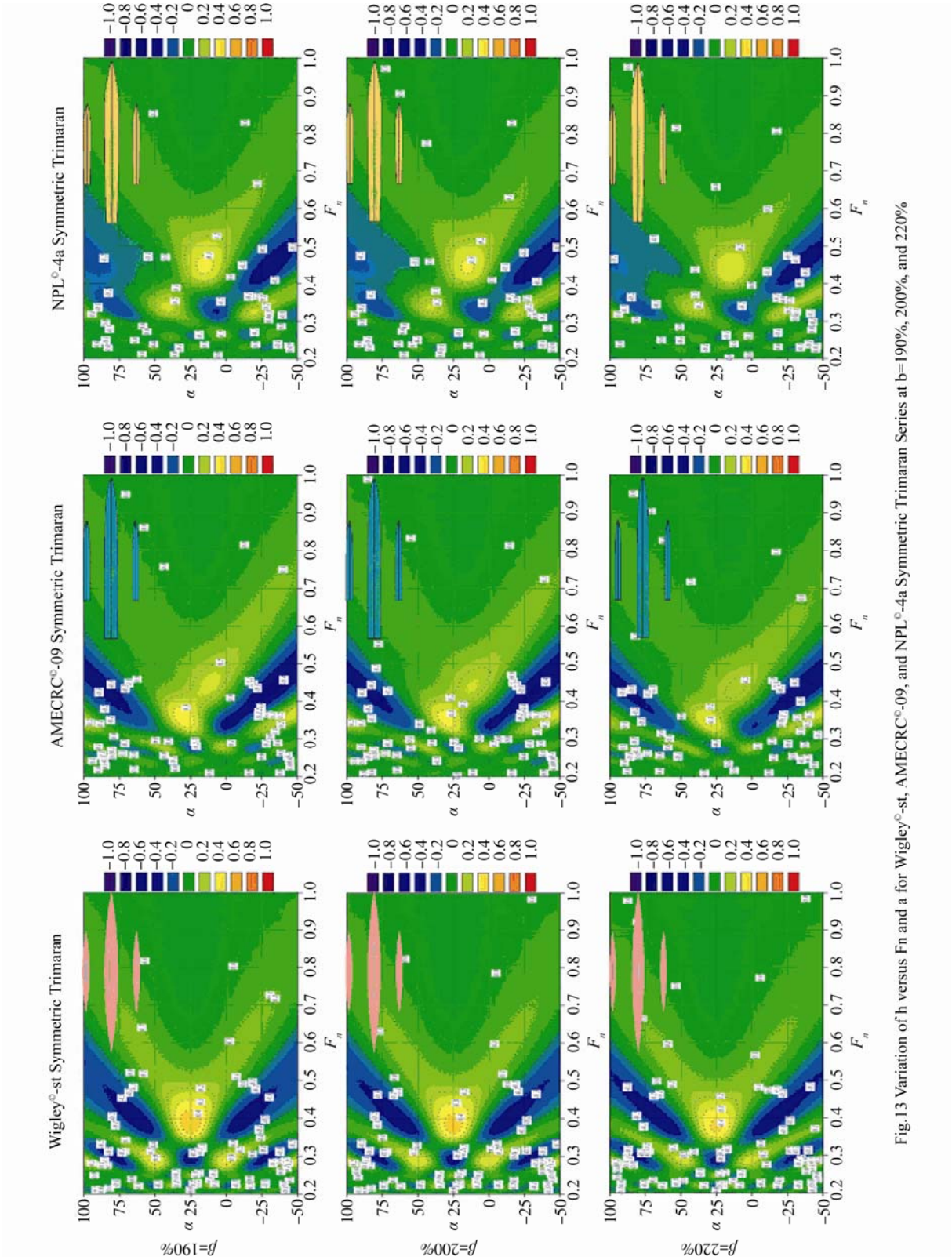

Fig.13 Variation of h versus Fn and a for Wigley©-st, AMECRC©-09, and NPL©-4a Symmetric Trimaran Series at b=190%, 200%, and 220%

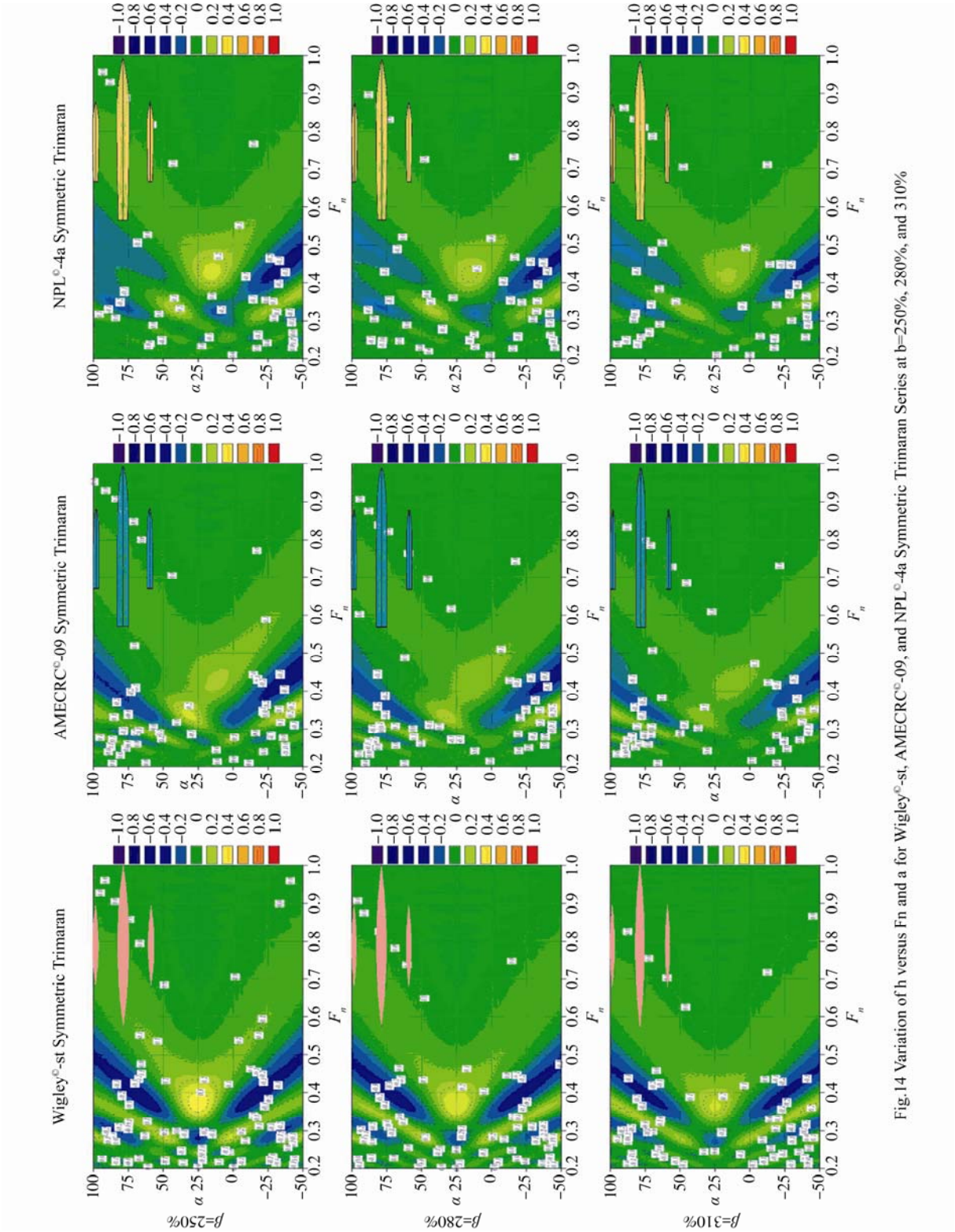

Fig.14 Variation of h versus Fn and a for Wigley©-st, AMECRC©-09, and NPL©-4a Symmetric Trimaran Series at b=250%, 280%, and 310%

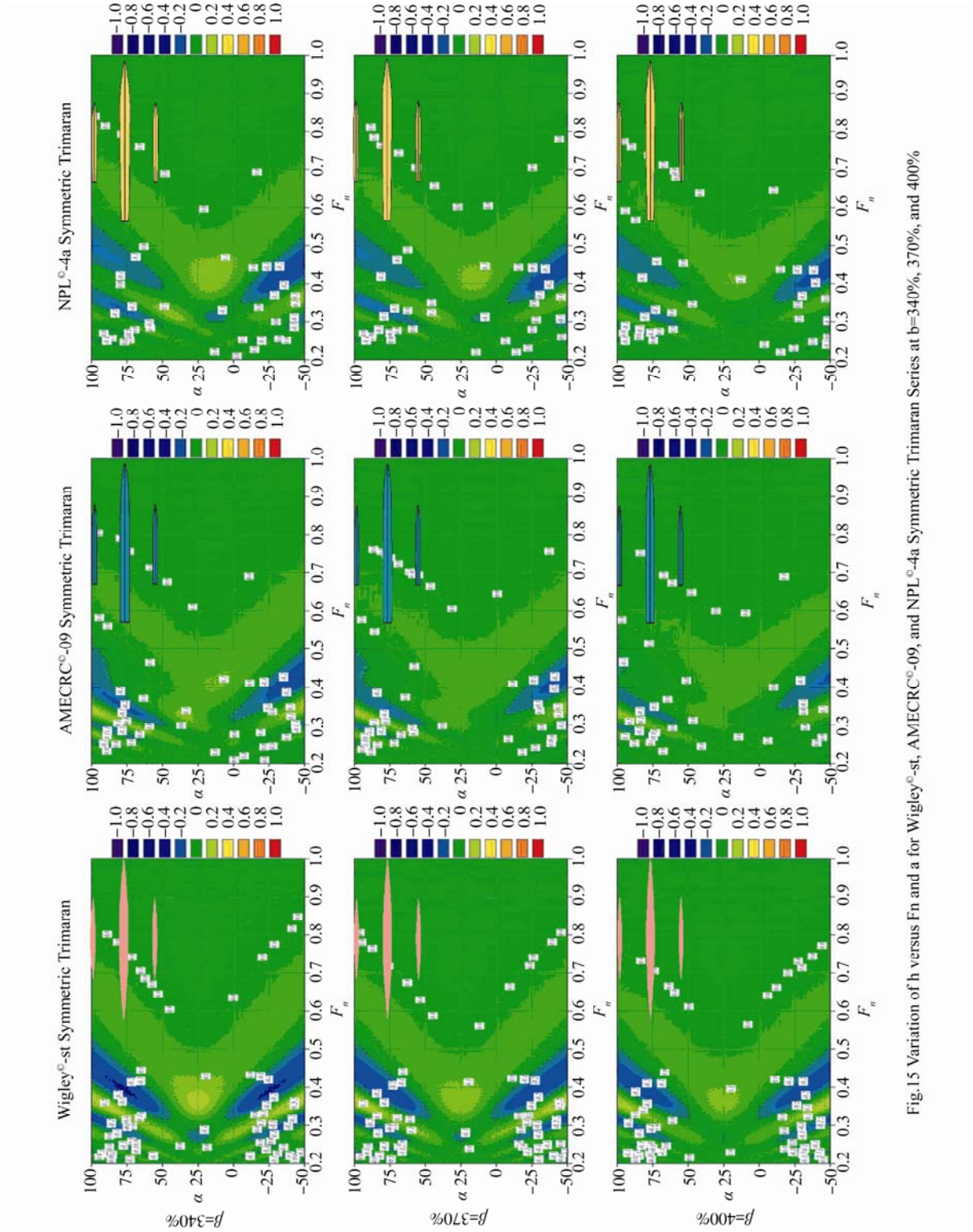

Fig.15 Variation of h versus Fn and a for Wigley©-st, AMECRC©-09, and NPL©-4a Symmetric Trimaran Series at b=340%, 370%, and 400%

The latter methods include the 2−D SBM, experiments, and the 3−D potential flow panel method of ShipFlow©, already published by Mynard *et al.* (2008) as well as the numerical results of the Hullspeed© (2011) via the Tri-PL© macro. In such validation, the numerical results of Hullspeed© (2011) via the Tri-PL© macro seem to agree very well with the numerical results of Mynard *et al.* (2008) along the considered F_n interval $0.20 \le F_n \le 1.0$. The results highlight a substantial increase in C_{wtri} toward decreasing α for the same β, showing the influence of the hydrodynamic interference beneath the triple hulls. The situation is different with the ShipFlow© (2011), where the trend of its results seem to agree with that of the Hullspeed©

(2011) via the Tri-PL© macro over the interval $0.45 \le F_n \le 1.0$, but over-predicting C_{wtri} along the interval $0.30 \le F_n \le 0.45$. The numerical results of Hullspeed© (2011) via the Tri-PL© macro record a seemingly mismatched C_{wtri} which results in the different F_n zones with the experimental results of Mynard et al. (2008); matching the other two numerical results in recording a clear under-prediction of C_{wtri}.

The aforementioned numerical results differ from each other and from the experimental model due to the ways considered in manipulating the transom stern, the bow wave-breaking resistance, the viscous drag, the eddy formation, the forward thrust of the viscous pressure fields, the flow separation around the hull, the mutual interaction beneath the resistance components, and the rooster tail behind the model. Also, the reliability of the experimental results is principally based on the ship-model scaling, accuracy of the recording gauges, and the technicians' capabilities.

9 Analyses of the numerical results

Fig.12 shows the contours of η versus F_n and α for Wigley©-st, AMECRC©-09, and NPL©-4a symmetric trimaran series, respectively, at twelve arbitrarily selected separations, $\beta = 100\%$, 130%, 160%, 190%, 200%, 220%, 250%, 280%, 310%, 340%, 370%, and 400%. For comparative depiction of the three developed trimaran series, each row represents the contour of η for Wigley©-st, AMECRC©-09, and NPL©-4a trimarans at the specified β. For convenient interpretation of the graphs, the appropriate trimaran configuration at the arbitrarily selected β and $\alpha = +25\%$ appears therein.

A hollow represents a negative interference which is beneficial; i.e., the resistance of the corresponding trimaran configuration is less than the non-interfered resistances, whereas a hump signifies a positive interference which is detrimental. A flat contour indicates a zero interference which is idling (non-beneficial); i.e., the resistance of the corresponding trimaran configuration equals the non-interfered resistances. The interference effects may be reverted to the constructive/destructive interaction of the individually induced bi-wave systems, the wave-induced variations in the tri-wetted surface areas, and/or the induced mutual pressure gradients. Such interference effects almost vanish at higher separations, on the penalty of difficult docking and stiff transverse stability.

The pressure carrying the trimaran may be divided into hydrostatic and hydrodynamic. The hydrostatic pressure gives the buoyancy force, which is proportional to the submerged displacement volume of the trimaran; the hydrodynamic pressure depends on the flow around the hull and is approximately proportional to the ship speed squared. For $F_n \le 0.45$, the buoyancy force dominates relative to the hydrodynamic force, and the trimaran is termed displacement. For $0.45 \le F_n \le 1.0$, the hydrodynamic force dominates relative to the buoyancy force and the trimaran is termed semi-displacement. Generally, frictional resistance dominates at lower speeds, whereas, the wave-making resistance dominates as the speed increases. However, for a slender fine trimaran, as its wetted surface area increases, its frictional resistance increases too, and its wave-making resistance reduces at higher speeds.

At $\beta = 100\%$, a pattern of hollows (beneficial interference) and humps (detrimental interference) of η appears to be symmetric around $\alpha = +25\%$ for the Wigley©-st trimaran; it appears to be asymmetric for both the AMECRC©-09 and NPL©-4a trimarans.

Concerning the beneficial interference, two significant backward skewed hollows $\eta = -0.30$ (Wigley©-st trimaran) and $\eta = -0.40$ (AMECRC©-09 trimaran) extending over the intervals $0.39 \le F_n \le 0.505$, $-50\% \le \alpha \le -12.5\%$, $0.39 \le F_n \le 0.505$, $+62.5\% \le \alpha \le +100\%$ and $0.36 \le F_n \le 0.41$, $-3\% \le \alpha \le -15\%$, $0.375 \le F_n \le 0.49$, $+65\% \le \alpha \le +92\%$, respectively. The situation is different for the NPL©-4a trimaran, where three significant backward skewed hollows $\eta = -0.30$ extending over the intervals $0.35 \le F_n \le 0.36$, $+5\% \le \alpha \le +10\%$, $0.405 \le F_n \le 0.55$, $+72.5\% \le \alpha \le +100\%$ and $0.46 \le F_n \le 0.48$, $-35\% \le \alpha \le -30\%$. However, for the Wigley©-st trimaran, another three hollows, two backward skewed $\eta = -0.30$ at $\alpha = -25\%$, $+75\%$ and one $\eta = -0.40$ at $\alpha = +25\%$; all appear to concentrate around $F_n = 0.30$. Such triple hollows do not appear in the $\beta = 100\%$ graphs of either the AMECRC©-09 or NPL©-4a trimarans.

Concerning the detrimental interference, its pattern is totally different by moving between the three trimarans. For the Wigley©-st trimaran, four backward skewed humps, two humps of $\eta = +0.40$, and two humps of $\eta = +0.50$ appear to concentrate around $F_n = 0.29$ at $\alpha = -50\%$, $\alpha = +100\%$ and $F_n = 0.30$, $\alpha = -52.5\%$, $+2.5\%$, respectively. The first two humps extend over the intervals $0.28 \le F_n \le 0.31$, $-40\% \le \alpha \le -50\%$ and $0.28 \le F_n \le 0.31$, $+90\% \le \alpha \le +100\%$; whereas the second two humps extend over the intervals $0.285 \le F_n \le 0.325$, $-10\% \le \alpha \le +5.0\%$ and $0.285 \le F_n \le 0.325$, $+45\% \le \alpha \le +60.0\%$. Another significant hump $\eta = +0.50$ appears to concentrate around $F_n = 0.45$, $\alpha = +25\%$ in the displacement-to-semi-displacement transition zone and

extending over the interval $0.42 \le F_n \le 0.47$, $+20\% \le \alpha \le +30\%$. For the AMECRC©-09 trimaran, three significant backward skewed humps, one hump of $\eta = +0.50$ and two humps of $\eta = +0.30$ appear to concentrate around $F_n = 0.41$ at $\alpha = +26\%$ and $F_n = 0.35$ at $\alpha = -35\%$, $+100\%$, respectively. The first hump extends over the intervals $0.37 \le F_n \le 0.445$, $+20\% \le \alpha \le +32\%$; whereas the second two humps extend over the intervals $0.32 \le F_n \le 0.39$, $-50\% \le \alpha \le -30\%$ and $0.335 \le F_n \le 0.365$, $+88\% \le \alpha \le +100\%$. For the NPL©-4a trimaran, three significant backward skewed humps, one hump of $\eta = +0.40$ and two humps of $\eta = +0.30$ appear to concentrate around $F_n = 0.34$ at $\alpha = +40\%$, and $F_n = 0.34$, 0.52 at $\alpha = -27\%$, $+12.5\%$, respectively. The first hump extends over the intervals $0.335 \le F_n \le 0.355$, $+41\% \le \alpha \le +43\%$; whereas the second two humps extend over the intervals $0.315 \le F_n \le 0.37$, $-35\% \le \alpha \le -17.5\%$ and $0.425 \le F_n \le 0.605$, $+7\% \le \alpha \le +30\%$.

Few minor hollows $\eta = -0.10$, -0.20 and humps $\eta = +0.10$, $+0.20$ appear extending over unequal narrow intervals of α in the $\beta = 100\%$ graphs of the three trimarans. Such minor hollows and humps appear scattered in the displacement interval $0.20 \le F_n \le 0.30$ for the Wigley©-st and AMECRC©-09 trimarans; whereas it appear scattered in the displacement interval $0.20 \le F_n \le 0.32$ for NPL©-4a trimaran.

As β increases by moving the outriggers of the individual trimarans transversely outward the central main hull, the aforementioned three patterns of humps and hollows navigate toward the lower F_n in the displacement zone. In the three patterns of humps and hollows, the humps decay gradually till they become shallow. For the Wigley©-st trimaran, its pattern of humps and hollows keep its symmetry around $\alpha = +25\%$.

The end of the separation variation is declared by reaching $\beta = 400\%$, at which the behavior of the patterns of hollows and humps for the three trimarans is different.
For the Wigley©-st trimaran, four backward skewed hollows, two hollows of $\eta = -0.20$ and two hollows of $\eta = -0.10$ appear to extend over the intervals $0.35 \le F_n \le 0.46$, $-50\% \le \alpha \le -12.5\%$, $0.30 \le F_n \le 0.32$, $-49\% \le \alpha \le -38\%$, $0.23 \le F_n \le 0.25$, $-37.5\% \le \alpha \le -17.5\%$, and $0.21 \le F_n \le 0.24$, $-50\% \le \alpha \le -25\%$, respectively. Another four backward skewed hollows, represent mirror reflections of the first four hollows, appear to extend over the intervals $0.35 \le F_n \le 0.46$, $+62.5\% \le \alpha \le +100\%$, $0.30 \le F_n \le 0.32$, $+88\% \le \alpha \le +99\%$, $0.23 \le F_n \le 0.25$, $+67.5\% \le \alpha \le +87.5\%$, and $0.21 \le F_n \le 0.24$, $+75\% \le \alpha \le +100\%$, respectively. Also, a shallow hump $\eta = +0.10$ appears to cover the interval $0.335 \le F_n \le 0.395$, $+12.5\% \le \alpha \le +37.5\%$.

For the AMECRC©-09 trimaran, four shallow backward skewed hollows $\eta = -0.10$ appear to cover the intervals $0.345 \le F_n \le 0.485$, $+50\% \le \alpha \le -12.5\%$, $0.305 \le F_n \le 0.405$, $+60\% \le \alpha \le +100\%$, $0.27 \le F_n \le 0.31$, $+85\% \le \alpha \le +100\%$ and $0.44 \le F_n \le 0.48$, $+93\% \le \alpha \le +100\%$. Also, four shallow humps $\eta = +0.10$ appear scattered in the displacement interval $0.25 \le F_n \le 0.35$ and extending over unequal wide intervals of α.

For the NPL©-4a trimaran, three backward skewed hollows, one hollow of $\eta = -0.20$, and two hollows of $\eta = -0.10$ appear to extend over the intervals $0.395 \le F_n \le 0.47$, $+50\% \le \alpha \le -22\%$, $0.29 \le F_n \le 0.38$, $+55\% \le \alpha \le +100\%$ and $0.39 \le F_n \le 0.54$, $+55\% \le \alpha \le +100\%$, respectively. Another few minor backward skewed hollows $\eta = -0.10$ appear scattered in the displacement interval $0.20 \le F_n \le 0.30$ and extending over unequal wide intervals of α. Also, a shallow hump $\eta = +0.10$ appears to concentrate around $F_n = 0.41$ and $\alpha = +17\%$.

The patterns of the remaining η contours of the three trimarans show approximately smooth flat surface (non-beneficial) $\eta = 0.0$, indicating that the interaction effects at such separation configuration and the corresponding speed intervals have progressively died-out.

The interested researchers may refer to Table 1, Appendix I, in which all recommended locations α and β of the side hulls with respect to the main hull along the whole intervals $-50\% \le \alpha \le +100\%$ and $100\% \le \beta \le 400\%$ at the beneficial η corresponding to the required design F_n for the Wigley©-st, AMECRC©-09 and NPL©-4a trimarans respectively are tabulated.

10 Conclusions and recommendations

This paper numerically investigated the influence of separation variation of the outriggers on the hydrodynamic performance of three trimaran series. Brief investigations of the principal conclusions that may be aggregated from the numerical calculations and analysis are:

1) The computer macro Tri-PL© - as it is - represents a powerful design tool capable for locating the design

alternatives having beneficial interferences, minimizing the detrimental interferences (as practical as possible), and avoiding the design alternatives having non-beneficial/detrimental interferences.

2) This comparative analysis of the three trimaran series proves – with no doubt - that the hydrodynamic interference η is generally less sensitive to β than α up to a certain shoulder speed which is dependent on α, β and the immersed geometry of the trimaran. Above such shoulder speed the influence of α and/or β on the hydrodynamic interference η is insignificant.

3) This comparative analysis proves that SBM with a virtual transom correction offers a realistic estimation of the trimaran wave-making resistance over a wide speed range $0.20 \le F_n \le 1.0$, and hence provides a vital practical design tool for sophisticated parametric studies.

4) The trimaran model NPL©-4a with the largest transom area $A_t = 7.037\text{m}^2$ records higher total resistance than the other two models of Wigley©-st $A_t = 0.0\text{m}^2$ and AMECRC©-09 $A_t = 5.496\text{m}^2$, even if it has a small wave resistance.

5) The influence of the extent and rate of the transom wetness/dryness as well as the generated transom eddies on the total resistance and hence on the trimaran hydrodynamic performance already prepared and will be discussed thoroughly in a sooner future publication.

Acknowledgement

The corresponding author would like to express his grateful thanks to the Maxsurf© team, Formation Design Systems, Australia, and SigmaPlot© team, Systat Software Inc., UK; for their sincere help and support. The views, opinions, analysis and conclusions expressed herein are those of the corresponding author, for which he alone should be held responsible.

Nomenclature

Alphabetic Symbols

A_M	Maximum transverse section area of the parent model
A_S	Wetted surface area of the parent model
$A_{S_{cnt}}$	Wetted surface area of the main hull
$A_{S_{out}}$	Wetted surface area of the side hull
$A_{S_{tri}}$	Wetted surface area of the trimaran
A_W	Waterplane area of the parent model
BM_L	Longitudinal metacentric radius of the parent model
BM_T	Transverse metacentric radius of the parent model
B_W	Waterplane maximum breadth of the parent model
B_W/d_M	Waterplane maximum breadth-to-draft ratio of the parent model
$C_{a_{tri}}$	Correlation allowance of the trimaran, encompassing roughness allowance, particularities of the measuring device of the model basin, errors in the model-ship correlation line and the method.
C_B	Block coefficient of the parent model; $C_B = \Delta/\rho L_W B_W d_M$
$C_{f_{cnt}}$	Calm water friction resistance coefficient of the main hull
$C_{f_{out}}$	Calm water friction resistance coefficient of the side hull
$C_{f_{tri}}$	Calm water friction resistance coefficient of the trimaran
$C_{f_{tri-NI}}$	Calm water friction resistance coefficient of the non-interfered trimaran hulls
C_M	Maximum section area coefficient of the parent model; $C_M = A_M/B_W d_M$
C_P	Prismatic coefficient of the parent model; $C_P = \Delta/\rho L_W A_M$
$C_{r_{tri}}$	Calm water residuary resistance coefficient of the trimaran
$C_{r_{tri-NI}}$	Calm water residuary resistance coefficient of the non-interfered trimaran hulls
$C_{t_{cnt}}$	Calm water total resistance coefficients of the main hull
$C_{t_{out}}$	Calm water total resistance coefficients of the side hull
$C_{t_{tri}}$	Calm water total resistance coefficient of the trimaran
$C_{t_{tri-NI}}$	Calm water total resistance coefficients of the non-interfered trimaran hulls
$C_{v_{cnt}}$	Calm water viscous resistance coefficient of the main hull
$C_{v_{out}}$	Calm water viscous resistance coefficient of the side hull
$C_{v_{tri}}$	Calm water viscous resistance coefficient of the trimaran
$C_{v_{tri-NI}}$	Calm water viscous resistance coefficient of the non-interfered trimaran hulls
C_W	Waterplane area coefficient of the parent model; $C_W = A_W/L_W B_W$
$C_{w_{cnt}}$	Calm water wave-making resistance coefficient of the main hull
$C_{w_{out}}$	Calm water wave-making resistance coefficient of the side hull
$C_{w_{tri}}$	Calm water wave-making resistance coefficient of the trimaran
$C_{w_{tri-NI}}$	Calm water wave-making resistance coefficient of the non-interfered trimaran hulls
D_M	Maximum depth of the parent model
d_M	Maximum draft of the parent model
F_n	Froude number of the main central hull
KB	Vertical center of buoyancy of the parent model
LCB	Longitudinal center of buoyancy of the parent model expressed as percentage of its waterplane length
LCF	Longitudinal center of floatation of the parent model expressed as percentage of its waterplane length
$L_{w_{cnt}}$	Waterplane length of the main hull
$L_{w_{out}}$	Waterplane length of the side hull
L_W	Waterplane length of the parent model
L_W/B_W	Waterplane length-to-maximum breadth ratio of the parent model

$L_W/\nabla^{1/3}$	Slenderness ratio of the parent model
m	Number of the slender body mesh contours (transverse sections)
$MCT1.0cm$	Moment causing trim 1.0 cm of the parent model
n	Number of the slender body mesh points (waterlines)
$R_{e_{cnt}}$	Reynolds number of the main hull
$R_{e_{out}}$	Reynolds number of the side hull
$R_{f_{tri}}$	Calm water friction resistance of the trimaran
$R_{r_{tri}}$	Calm water residuary resistance of the trimaran
$R_{t_{tri}}$	Calm water total resistance of the trimaran
$R_{v_{tri}}$	Calm water viscous resistance of the trimaran
$R_{w_{tri}}$	Calm water wave resistance of the trimaran
t	Temperature of the salt water
TPC	Tonne per centimeter of the parent model
U	Velocity of the trimaran
x	Stagger measured as the longitudinal coordinate of the aft perpendicular of the side hulls with respect to the origin
y	Separation measured as the transverse coordinate of the central plane of the side hulls with respect to the origin
$(1+k)_{cnt}$	Form factor of the main hull
$(1+k)_{out}$	Form factor of the side hull

Greek Symbols

α	Stagger expressed as percentages of the parent model waterplane length
β	Separation expressed as percentages of the parent model waterplane maximum breadth
Δ	Displacement of the parent model; $\Delta = C_B \rho L_W B_W d_M$
ε	Salinity of the salt water
η	Hydrodynamic interference factor
θ_D	Dead-rise angle at $50\% L_W$ of the parent model
θ_E	Half angle of entrance of the parent model
λ	Trimaran main-to-side hulls scale factor
ρ	Mass density of the salt water
ν	Kinematic viscosity of the salt water

References

Bailey D (1976). The NPL High speed round bilge displacement hull series. marine technology monograph. *The Royal Institute of Naval Architects (RINA)*, 4.

Batchelor G (1959). A proposal concerning wakes behind bluff bodies at large Reynolds numbers. *Journal of Fluid Mechanics*, **6**, 547-567.

Bojovic P (1995). AMECRC Systematic series calm water testing results. Australian Maritime Engineering Cooperative Research Centre, Report AMECRC IR 95/5, 1-93.

Bojovic P, Goetz G (1996). Geometry of AMECRC systematic series. Australian Maritime Engineering Cooperative Research Centre, Report AMECRC IR 96/6, 1-37.

Cone CD (1963). The aerodynamic design of wings with cambered span having minimum induced drag. Langley Research Center, Virginia, United States, NASA Technical Report No. TR R-152.

Couser P, Wellicome J, Molland A (1998). An improved method for the theoretical prediction of the wave resistance of transom-stern hulls using a slender body approach, *International Shipbuilding Progress*, **45** (444).

Doctors L (1995). A practical method of prediction of ship resistance for displacement vessels. *International Symposium on Practical Design of Ships and Mobile Units (PRADS'95)*, Society of Naval Architects of Korea, Korea, 1, 648-659.

Doctors L, Day A (1997). Resistance prediction for transom-stern vessels. *International Conference on Fast Sea Transportation (FAST'97)*, Australia, **2**, 743-750.

Doctors L, Beck R (2005). The separation of the flow past a transom stern. *International Conference on Marine Research and Transportation (ICMRT'05)*, Italy, 14.

Doctors L (2006). Investigation of the free-surface and resistance of transom-stern vessels. *Pacific International Maritime Conference (PIMC'06)*, Australia, 196-205.

Doctors L (2006). Influence of the transom-hollow length on wave resistance. *International Workshop on Water Waves and Floating Bodies (IWWWFB'21)*, England, 4.

Eggers K (1955). Resistance components of two-body ships, Jahrbuch der Schiffbautechnischen Gesellschaft, 49.

Hanhirova K, Rintala S, Karppinen T (1995). Preliminary resistance prediction method for fast mono-and-multihull vessels. *International Symposium on High Speed Vessels for Transport and Defence*, Royal Institution of Naval Architects (RINA), England, **6**, 1-17.

Hullspeed© (2011). Formation Design Systems Pty Ltd., Available at: http://www.formsys.com/.

Insel M (1990). An investigation into the resistance components of high speed displacement catamarans, Ph. D. thesis, University of Southampton.

Marwood W, Bailey D (1969). Design data for high-speed displacement hulls of round-bilge form. Ship Report 99, National Physical Laboratory.

Maxsurf© (2011). Formation Design Systems Pty Ltd., Available at: http://www.formsys.com/.

Michell J (1898). The wave resistance of a ship. *Philosophical Magazine*, England, **5** (45), 106-123.

Michlet© (2010), Wave resistance prediction software, Available at: http://www.cyberiad.net.

Mynard T, Sahoo P, Mikkelsen J, McGreer D (2008). Numerical and experimental study of wave resistance for trimaran hull forms. Australian Maritime College, Australia, 117-132.

Newman J (1999). *Marine hydrodynamics*. The Massachusetts Institute of Technology (MIT) Press.

Robards S, Doctors L (2003). Transom-hollow prediction for high-speed displacement vessels. *International Conference on Fast Sea Transportation (FAST'03)*, Italy, **1** (A), 19-26.

ShipFlow©, flowtech international AB, Available at: http://www.flowtech.se/, Accessed, **2**, 2011.

SigmaPlot© (2006). Systat Software Inc., Available at: http://www.systat.com/.

Sinha S (1981). Backward facing step flow experiments. *AIAA Journal*, **19**, 1527-1530.

Tuck E, Luzauskas L, Scullen D (1999). Sea wave pattern evaluation. part 1 report: primary code and test results (Surface vessels), Applied Mathematics Department, the University of Adelaide.

Visual Basic for Applications© (2010). Microsoft© Corp., Available at: http://www.Microsoft.com/.

Wehausen J, Laitone E (1960). Surface waves. *Encyclopedia Of Physics*, **9**, Berlin-Gottingen-Heidelberg, Springer-Verlag.

Wehausen J (1971). The motion of floating bodies. *Annual Revision of Fluid Mechanics*, **3**, 237-268.

Wigley W (1934). A comparison of experimental and calculated wave profiles and wave resistances for a form having parabolic waterlines. *Royal Society London*, Ser. A, **144**(851), 144–159.

(1957). Skin friction and turbulence. *International Towing Tank Conference* (ITTC'57), Madrid.

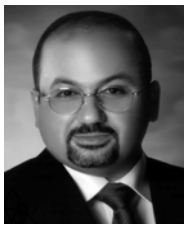

Dr. Khaled Hafez: Ph. D. degree (2002) in Civil Engineering, Architecture and Marine Technology, Department of Naval Architecture and Ocean Engineering, Faculty of Engineering, Yokohama National University, Japan. M. Sc. degree (1995) and B. Sc. "Distinction with Honor degree" (1991) in Naval Architecture and Marine Engineering, Faculty of Engineering, Alexandria University, Egypt. Currently, an Assistant Prof. (Lecturer) at the Department of Naval Architecture and Marine Engineering, Faculty of Engineering, Alexandria University, Egypt. Interested in Hydro-elasticity of Marine Structures, Hydrodynamics of Marine Structures, Wave-Ship Interaction, Computational Fluid Dynamics (CFD), Computer-Aided Ship Design (CAD), Naval Architecture and Ocean Engineering.

Abdel-Rahman El-Kot: B. Sc. degree (2011) in Naval Architecture and Marine Engineering, Faculty of Engineering, Alexandria University, Egypt. Interested in Ship Hydrodynamics.

Appendix I

Hydrodynamic Performance Particulars of Wigley©-st, AMECRC©-09 and NPL©-4a Trimarans

F_n	Wigley©-st			AMECRC©-09			NPL©-4a		
	α	β	η	α	β	η	α	β	η
0.20	86	100	-0.265172463	-37	110	-0.132975807	-18	200	-0.112128907
0.22	25	210	-0.262873591	73	140	-0.108095178	-50	230	-0.112584899
0.24	11	250	-0.163966614	75	100	-0.210172336	3	100	-0.162275938
0.26	25	310	-0.142245805	95	200	-0.171003923	23	190	-0.165560609
0.28	73	100	-0.33923792	24	160	-0.258614016	-14	140	-0.161952097
0.30	25	100	-0.414883957	100	380	-0.171879388	5	220	-0.180899764
0.32	25	100	-0.320883789	0	210	-0.262439605	7	180	-0.291582176
0.34	-3	280	-0.244324587	-2	170	-0.376929798	7	150	-0.341935858
0.36	-7	250	-0.337077102	-6	120	-0.437035852	5	130	-0.322392053
0.38	61	230	-0.37337761	-9	100	-0.452048531	80	100	-0.272951299
0.40	65	220	-0.369257793	73	100	-0.439833259	-21	210	-0.29793207
0.42	72	220	-0.349197142	76	100	-0.444269823	-25	190	-0.346523064
0.44	83	100	-0.334287713	80	100	-0.43651806	-28	170	-0.360915591
0.46	87	100	-0.326364973	83	100	-0.420977163	-30	160	-0.352959692
0.48	93	100	-0.316457673	87	100	-0.404458164	87	100	-0.348641835
0.50	95	100	-0.303831716	91	100	-0.387541944	91	100	-0.338824411
0.52	100	230	-0.292683535	95	100	-0.370471344	95	100	-0.327012636
0.54	100	210	-0.279687923	99	100	-0.353748738	99	100	-0.31369811
0.56	100	190	-0.2656987	100	100	-0.337198355	100	100	-0.299870857
0.58	100	180	-0.25071573	100	100	-0.316588042	100	100	-0.278834096
0.60	100	160	-0.238663868	100	100	-0.29367097	100	100	-0.252868621
0.62	100	150	-0.226474342	-50	110	-0.274855131	100	100	-0.226874486
0.64	100	140	-0.216560889	-50	100	-0.262226714	100	100	-0.203779403
0.66	100	130	-0.208222854	-50	100	-0.248319869	-50	110	-0.185786726
0.68	100	120	-0.201432661	-50	100	-0.230622356	-50	100	-0.177170406
0.70	100	110	-0.194670865	-50	100	-0.209843176	-50	100	-0.170205376
0.72	100	110	-0.18908496	-50	100	-0.185144411	-50	100	-0.161360052
0.74	100	100	-0.185764518	-50	100	-0.156430036	-50	100	-0.152252517
0.76	100	100	-0.179883292	-50	100	-0.126727962	-50	100	-0.141390923
0.78	100	100	-0.167174802	-50	100	-0.094888464	-50	100	-0.127129996
0.80	100	100	-0.152970472	-50	100	-0.065252698	-50	100	-0.110664466
0.82	100	100	-0.133870938	20	150	-0.04288625	-50	100	-0.092913965
0.84	100	100	-0.113060592	19	160	-0.046367944	100	100	-0.082398209
0.86	100	100	-0.090494769	18	150	-0.046975409	100	100	-0.081040065
0.88	100	100	-0.069693782	19	150	-0.048720787	100	100	-0.081600108
0.90	25	140	-0.053178938	20	140	-0.049468739	100	100	-0.075487888
0.92	25	140	-0.053200889	17	140	-0.050704627	100	100	-0.068542468
0.94	25	130	-0.054100903	17	130	-0.053085412	100	100	-0.059309395
0.96	25	130	-0.05415906	19	110	-0.051217048	18	140	-0.050477398
0.98	25	120	-0.054477404	19	110	-0.054512288	19	160	-0.048690554
1.00	25	120	-0.053113215	18	120	-0.052973509	19	150	-0.050746755